

The Investigation of the Weak Link Behavior in the Niobium (Nb) Doped $\text{Bi}_{1.6}\text{Pb}_{0.4}\text{Sr}_2\text{Ca}_2\text{Cu}_3\text{O}_\delta$ Superconductor

M. Jafari · H. Sedghi · A. Esmaili

Received: 2 June 2013 / Accepted: 28 June 2013 / Published online: 28 July 2013
© Springer Science+Business Media New York 2013

Abstract The Nb substitution effect on structural, DC electrical resistivity, and AC susceptibility properties of polycrystalline $\text{Bi}_{1.6}\text{Pb}_{0.4}\text{Sr}_2\text{Ca}_2\text{Cu}_3\text{O}_\delta$ samples is investigated. The behavior of weak link and intergranular coupling in the substituted samples is discussed. While the Bi-2223 phase concentration increases in the X-ray diffraction (XRD) pattern, the intragrain transition temperature remains nearly unchanged in the substituted samples. The intergrain transition temperature is changed with Nb substitution.

Keywords High-temperature superconductivity · Bi-base · Nb doped · Susceptibility · Critical current · Arrhenius plot

1 Introduction

Since the discovery of high-temperature superconductors (HTSCs) much effort has gone into understanding their supercurrent behavior in grain boundaries [1–3]. Due to the low coherence length of HTSCs, weak links and their alignments play an important role in the attenuation behavior of transport current, especially in the presence of external magnetic field. In HTSCs, sample preparation conditions such as heat treatment, impurity substitutions, and structural imperfections could change the behavior of weak links.

The Bi-based superconductor system with the generalized $\text{Bi}_2\text{Sr}_2\text{Ca}_{n-1}\text{Cu}_n\text{O}_{2n+4+y}$ formula has three distinct superconducting phases with different number of CuO_2 planes corresponding to different n values. These phases

are Bi-2201 ($n = 1$), Bi-2212 ($n = 2$) and Bi-2223 ($n = 3$) having transition temperatures of 20, 90 and 110 K, respectively [4, 5]. Among these phases, the creation of the Bi-2212 phase is thermodynamically stable over a large scale of temperature. Takano et al. have found that the partial lead substitution for bismuth could increase the volume fraction of the Bi-2223 phase [6], but after more than two decades, the formation of pure Bi-2223 phase is still an open subject in the field of Bi-based superconductors.

In this work, we have investigated the effect of Nb substitution for bismuth. Among the periodic table elements, the pure Nb is a unique type-II superconductor [7]. This property, and empty 4d level in the niobium oxide, encouraged us to choose this element for substitution [8]. We have used also magnetic susceptibility as a contactless method and Bean's critical state model to investigate the weak-link behavior of the substituted samples.

2 Experimental

Polycrystalline $(\text{Bi}_{1.6-x}\text{Nb}_x\text{Pb}_{0.4})\text{Sr}_2\text{Ca}_2\text{Cu}_3\text{O}_{10+y}$ samples (where $x = 0.0, 0.02, 0.06, 0.15, 0.35$) were prepared by a conventional solid-state reaction method using Bi_2O_3 , PbO , SrCO_3 , CaCO_3 , CuO , and Nb_2O_5 3N powders. The components were thoroughly mixed in the required proportions for each sample and calcined at 815 °C in air for 15 hours. In the second process, reground and pelletized samples were synthesized at 750 °C for 24 hours and then at 848 °C for 96 hours. In the final process, the temperature of the samples was reduced to the room temperature by furnace cooling. The resistivity measurements were carried out by the standard four-probe method using a low frequency/low AC current (65 Hz/2 mA). Electrical contacts

M. Jafari (✉) · H. Sedghi · A. Esmaili
Department of Physics, University of Urmia, 11 km Sero Road,
P.O. Box 165, Urmia, Iran
e-mail: jafari.ph1985@gmail.com

Fig. 1 The XRD patterns of the Nb-doped samples

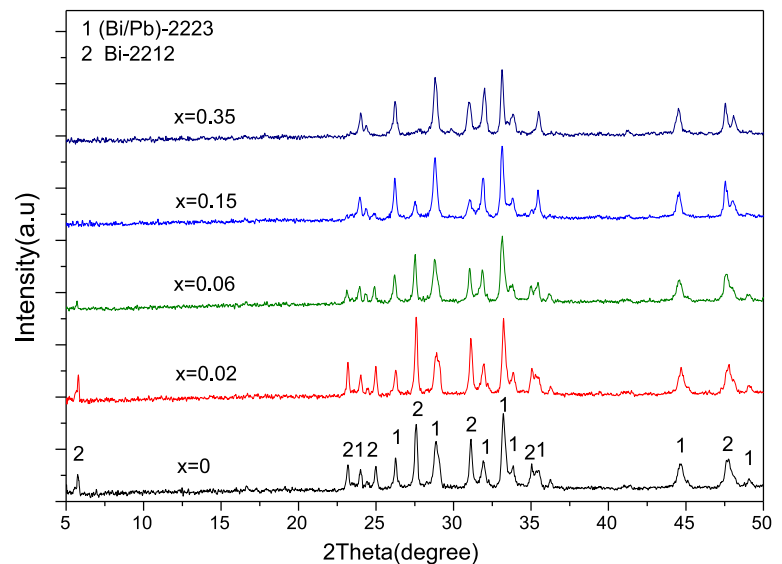


Table 1 XRD results for the Bi-2223 and Bi-2223 phase concentration in Nb substituted samples. The values of critical temperatures obtained from the resistivity measurements. The number of samples is defined in the first column

Sample	Nb concentration	Bi-2223 (%)	Bi-2212 (%)	T_c^{onset}	$T_c^{\text{offset}} (R=0)$
N_0	0	56.64	43.36	107.2	103.3
N_1	0.02	53.73	46.27	105.7	102.7
N_2	0.06	59.86	40.14	106.5	103.4
N_3	0.15	81.34	18.66	106.4	101.3
N_4	0.35	83.70	16.30	106.4	96.3

were made using conducting silver paint. Finally, the structure of the samples was examined using X-ray diffractometer (XRD) with (CuK α) source in the range $2\theta = 5\text{--}50$. The AC susceptibility measurements were performed using a Lake Shore susceptometer.

3 Results and Discussion

Figure 1 shows that the phases belonging to Bi-2223 and Bi-2212 are the major phases in the X-ray diffraction (XRD) pattern of samples. The volume fraction of the phases could be estimated as [9, 10]:

$$\text{Bi-2223(\%)} \approx \frac{\sum I(\text{Bi-2223})}{\sum I(\text{Bi-2223}) + \sum I(\text{Bi-2212})} \times 100, \quad (1)$$

$$\text{Bi-2212(\%)} \approx \frac{\sum I(\text{Bi-2212})}{\sum I(\text{Bi-2223}) + \sum I(\text{Bi-2212})} \times 100. \quad (2)$$

As shown in Table 1, the volume fraction of Bi-2223 is increased with increasing the Nb concentration.

In Fig. 2, the temperature dependence of the resistivity (R – T) shows that all the samples show metallic behavior in the normal state, and except for N_2 sample the resistivity increases with the increase of Nb concentration. All the samples show a two-step transition in the temperature range above the Bi-2212 phase transition temperature (i.e. 85 K). This behavior may be related to grain boundaries and structural phase transition from Bi-2223 to Bi-2212 [11]. The first peak in resistivity derivative curve (dR/dT) and the temperature at which the resistivity falls to zero are attributed to intragrain (T_c^{onset}) and intergrain (T_c^{offset}) superconducting transition temperatures, respectively [12]. Consistent with the XRD results, the variation of resistivity tail and the partial decrease in the intergrain transition temperature confirm that Nb substitution reduces the Bi-2212 phase. The T_c^{onset} value remains almost constant in the substituted samples and one can conclude that Nb lies at the grain boundaries and reduces the intergranular coupling.

As shown in Figs. 3, 4, and 5 for N_0 , N_2 and N_4 samples, applying weak external magnetic field the resistivity curve extends to lower temperatures. The intensity of the applied magnetic field was 0.25 T.

In the figure, only the tail part of the resistivity curve is extended and it shows that only weak links are affected by such weak magnetic field. According to the thermally activated flux creep model (TAFC), broadening in the resistivity curves is due to the vortex motion in the presence of an external magnetic field [12]. Vortex motion and flux creep are directly proportional to weak links, applied magnetic field and temperature. We conclude that upon increasing Nb concentration the flux pinning energy decreases.

We found that the experimental results in the tail part of the resistivity follow the Arrhenius equation. The Arrhenius plots of the samples are shown in the insets of Figs. 3,

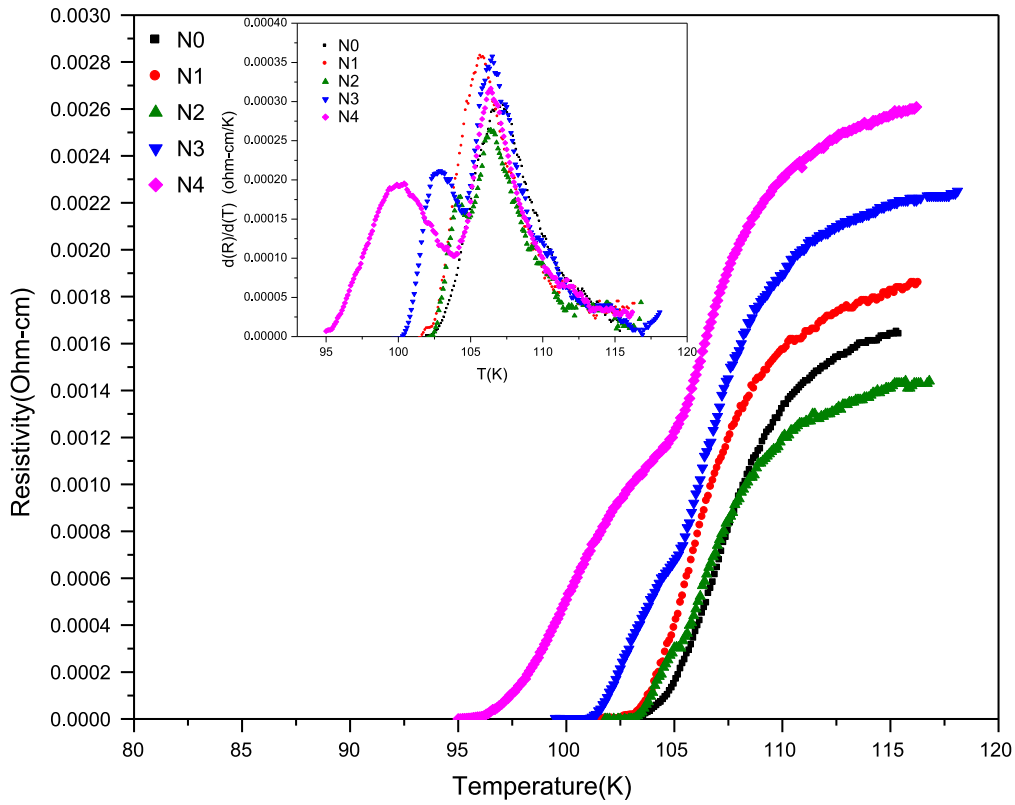


Fig. 2 The temperature dependence of the resistivity for all the samples. The *inset* shows the derivative of resistivity

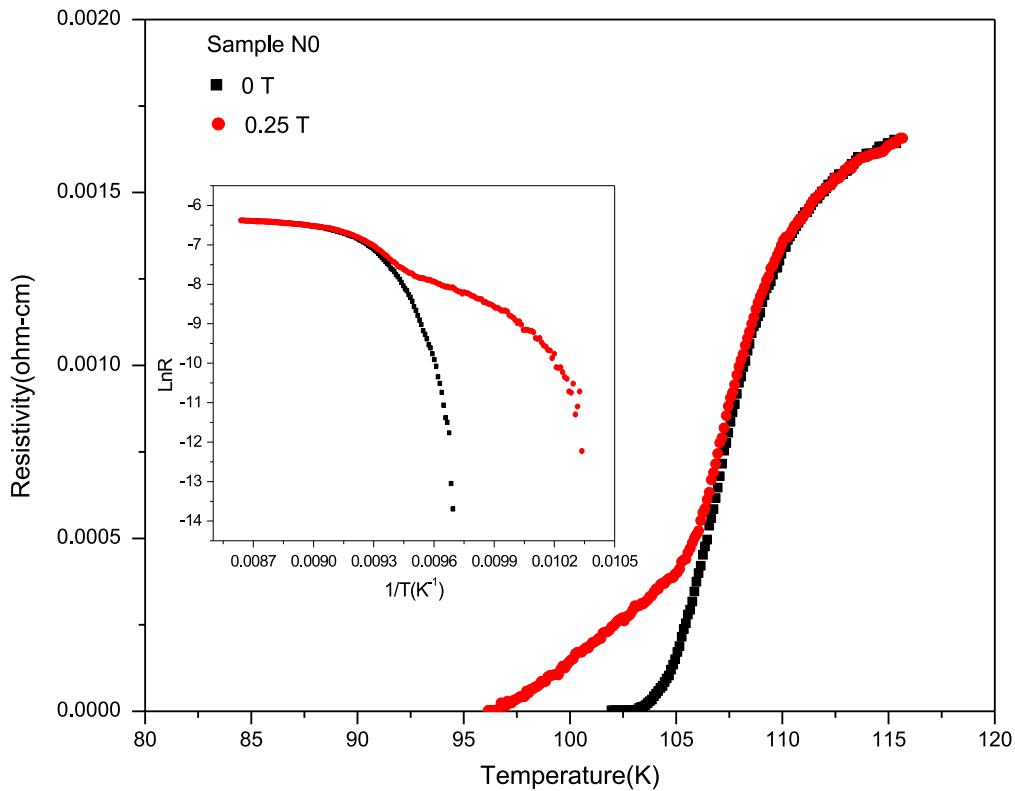


Fig. 3 Resistivity vs. temperature for the N_0 sample in the absence and presence of a weak magnetic field (0.25 T). The *inset* picture shows the Arrhenius plot of the resistivity for the N_0 sample

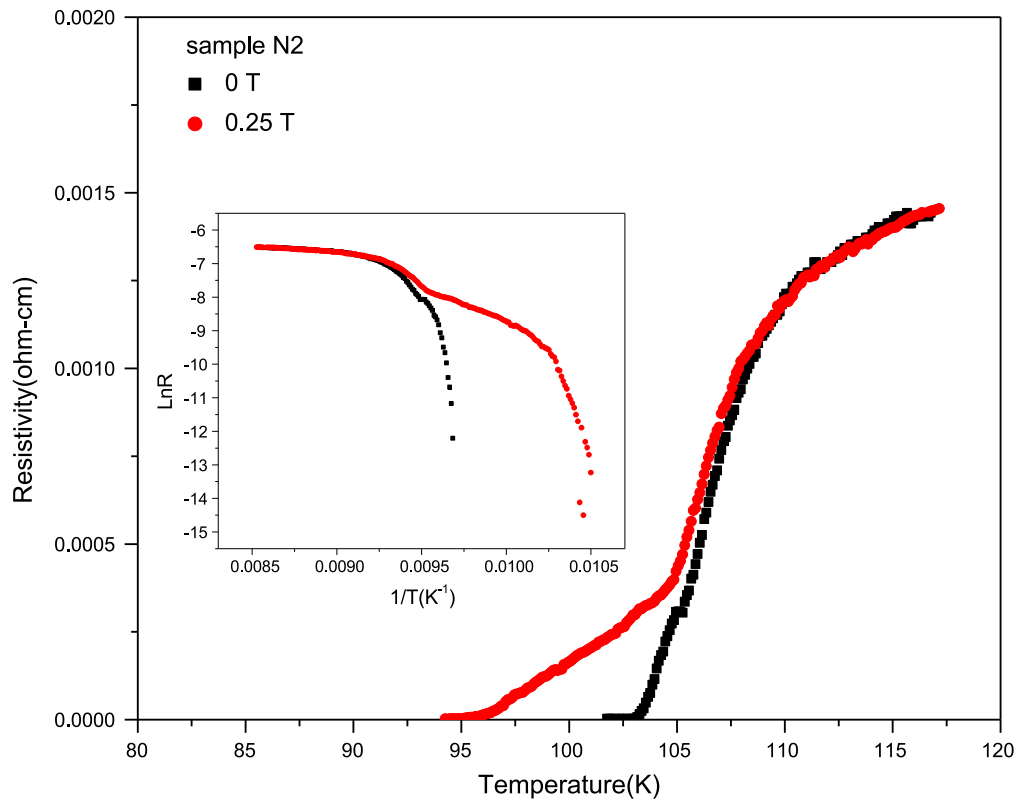


Fig. 4 Resistivity vs. temperature for the N_2 sample in the absence and presence of a weak magnetic field (0.25 T). The *inset* picture shows the Arrhenius plot of the resistivity for the N_2 sample

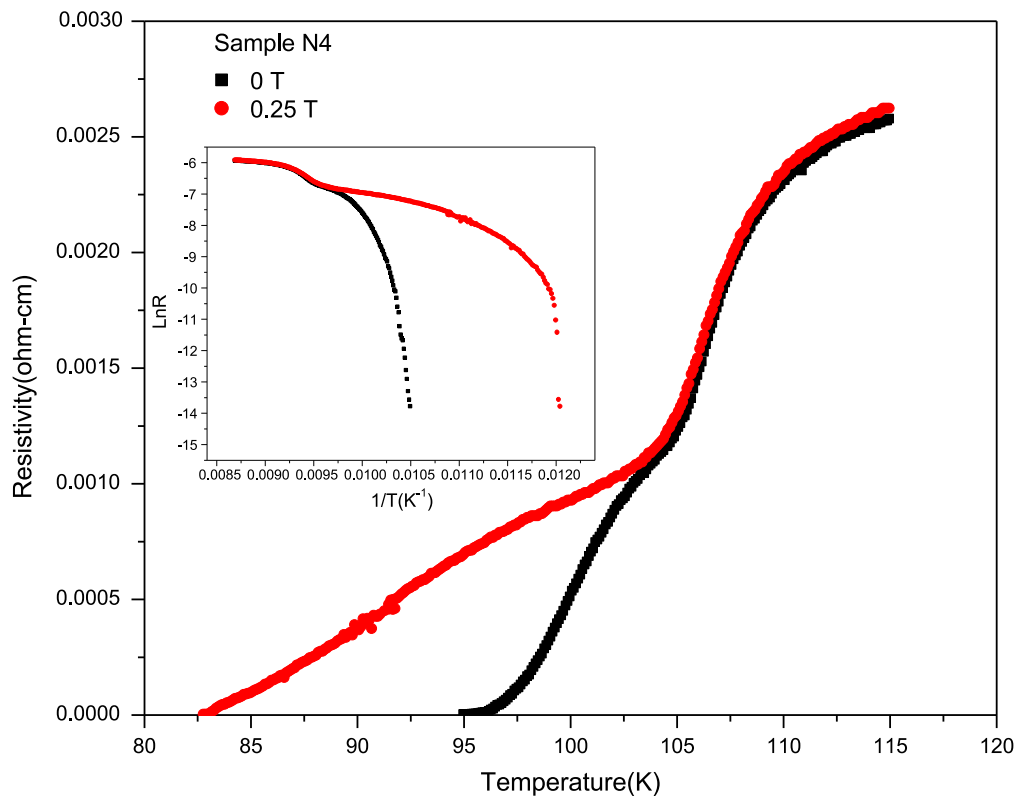


Fig. 5 Resistivity vs. temperature for the N_4 sample in the absence and presence of a weak magnetic field (0.25 T). The *inset* picture shows the Arrhenius plot of the resistivity for the N_4 sample

Fig. 6 In-phase components of AC magnetic susceptibility as a function of temperature for the N_0 , N_2 and N_4 samples. The inset picture shows in-phase component derivation as a function of temperature

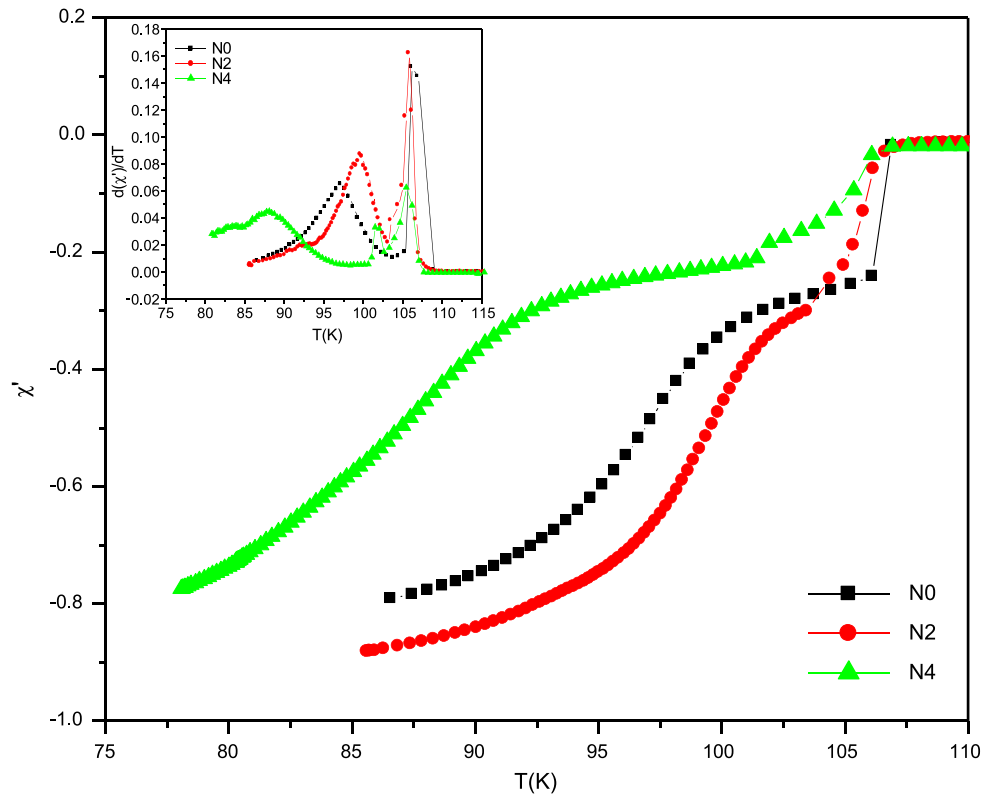


Table 2 The values of the flux pinning energy for N_0 , N_2 and N_4 samples

$B(T)$	Samples		
	N_0	N_2	N_4
0	933	591	430
0.25	760	500	415

Table 3 The results of transition temperatures

	T_c	T_{c_j}	T_p
N_0	106.11	97.11	97.64
N_2	105.75	99.61	99.61
N_4	105.63	87.97	87.35

4, and 5. It is used to determine the flux pinning energy [13, 14]:

$$\rho(H, T) = \rho_0 \exp(-U(H)/K_B T), \tag{3}$$

where U is the flux pinning energy which is weakly dependent on magnetic field, ρ_0 is a pre-factor which is nearly three orders of magnitude larger than normal state resistance, and K_B is the Boltzmann constant.

As expected for flux pinning energy, U has very small value in our samples and its value partially decreased with the increase of Nb concentration (Table 2).

Magnetic and superconducting properties of Nb substituted samples are also studied using AC susceptibility (χ_{ac})

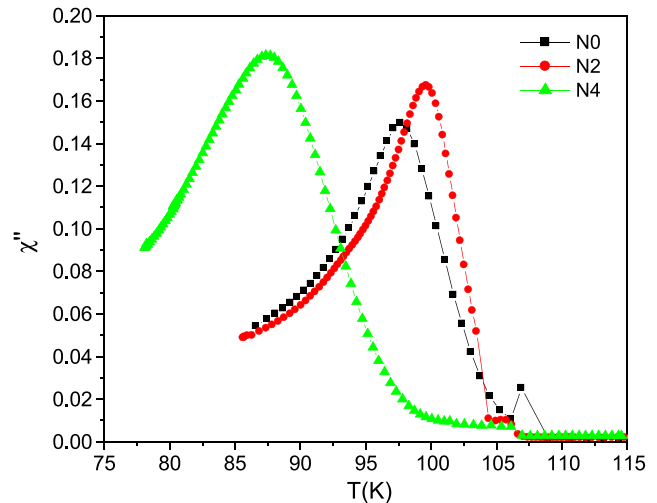


Fig. 7 Out-of-phase components of AC magnetic susceptibility as a function of temperature for the N_0 , N_2 and N_4 samples

measurement. The Bean’s critical state model was used to analyze the experimental χ_{ac} data between T_c and T_{c_j} [15, 16].

Figure 6 shows the temperature dependencies of the in-phase component of susceptibility (χ') for three selected samples in the applied AC field (30 A/m, 333 Hz) which was parallel with their long dimension. The hump of the real part of susceptibility shows the energy dissipation in the samples. In our polycrystalline samples, χ' shows two

Fig. 8 Temperature dependence of the AC susceptibility for the N_0 sample at 333 Hz frequency and various ac field amplitudes

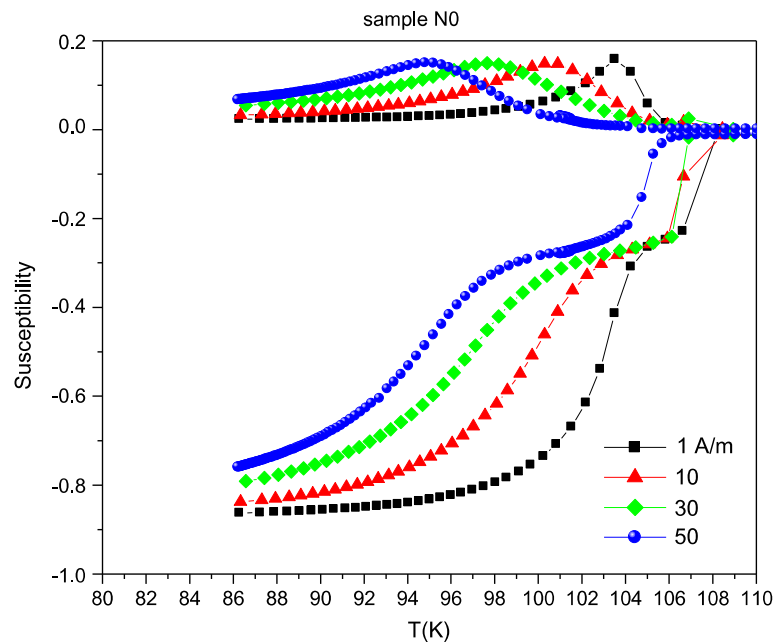
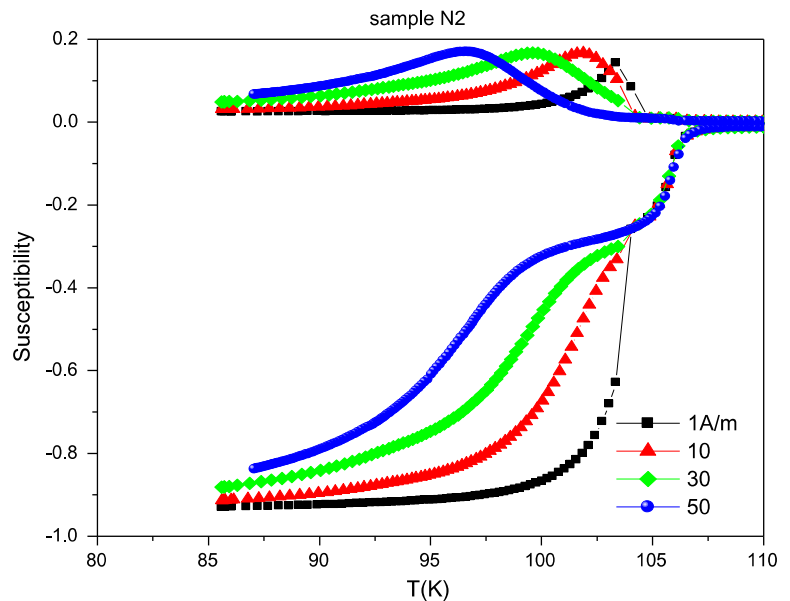


Fig. 9 Temperature dependence of the AC susceptibility for the N_2 sample at 333 Hz frequency and various ac field amplitudes



step drops in the temperatures below the diamagnetic transition onset temperature. The peaks in χ' derivative with respect to temperature display intragrain (T_c) and intergrain (T_{cj}) superconducting transition temperatures (the inset of Fig. 6). The first and second drops arise from the superconducting transition within grains and the superconducting coupling between grains, respectively. The decoupled grains below T_{cj} become well coupled in the temperature range between T_c and T_{cj} and equal to a zero-phase difference as a phase-lock occurs across the intergranular junctions.

As shown in Table 3, the T_c is about 106 K for undoped sample and remains nearly constant in substituted samples,

but T_{cj} has changed in the substituted samples. It shows that the intergranular coupling between grains has been increased for the sample of N_2 .

Figure 7 shows the temperature dependencies of the out-of-phase part of ac susceptibility (χ''). The broad peak in lower temperature and the other one below the onset of the diamagnetic temperature are attributed to the flux penetration into the intergranular region and the type of superconducting grains, respectively. The AC loss for N_2 occurs at higher temperature in comparison with two other samples.

Figures 8, 9, and 10 display the temperature dependencies of χ' and χ'' for the N_0 , N_2 , N_4 samples with various ac field amplitudes. The χ' and χ'' have no ac mag-

Fig. 10 Temperature dependence of the AC susceptibility for the N_4 sample at 333 Hz frequency and various ac field amplitudes

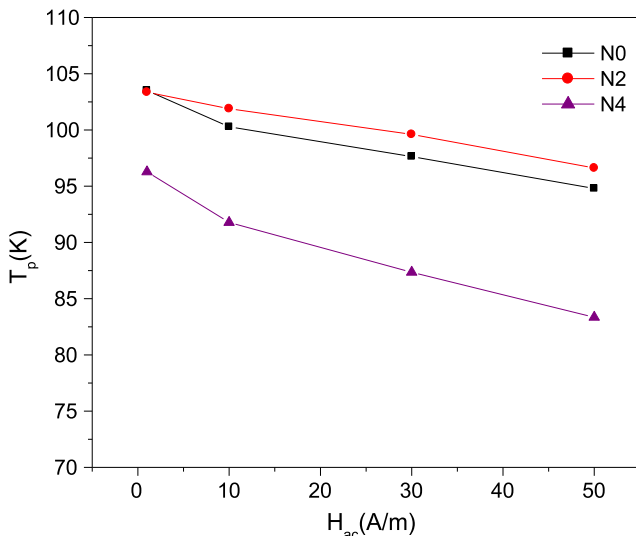
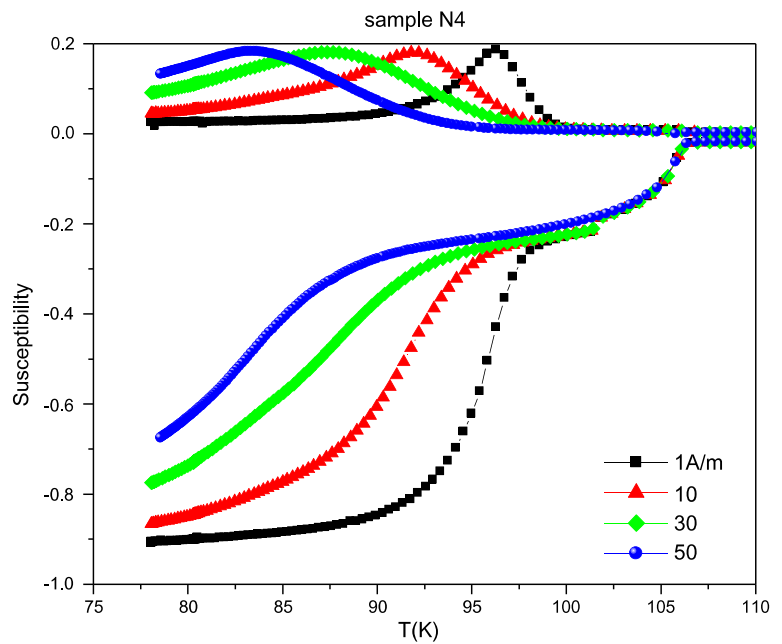


Fig. 11 The variation of temperature with AC field amplitude for the N_0 , N_2 and N_4 samples

netic field (H_{ac}) dependence between T_{c2} and T_{c1} but the superconducting transition temperature region is broadened below T_{c2} with the increase of H_{ac} . The χ'' hump temperature (T_p) shifts to lower temperature in the samples but its peak height remains nearly unchanged. The shift degree for N_4 sample is much bigger than for the other two samples. The field amplitude effect on χ' intergranular component for sample N_4 is also bigger than for the other two samples. The shift value is a function of H_{ac} and it is proportional to the strength of the pinning force.

The variation of T_p versus H_{ac} is shown in Fig. 11. The critical current density at T_p could be estimated using the

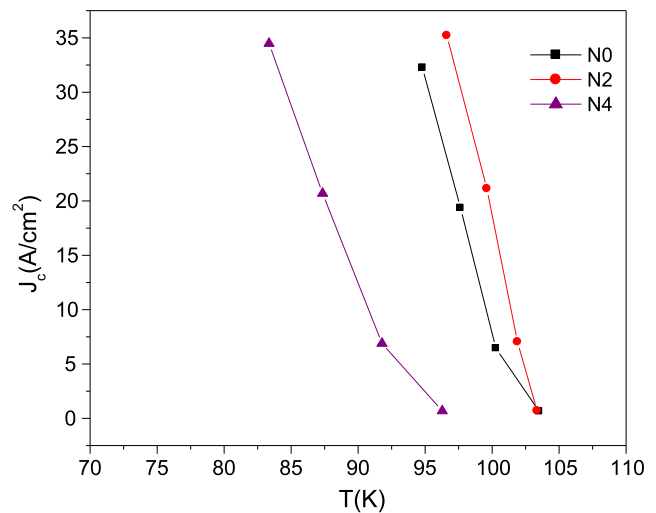


Fig. 12 The variation of J_c with temperature for the N_0 , N_2 and N_4 samples

Beans model:

$$J_c = \frac{H_{ac}}{(ab)^{1/2}},$$

where $a \times b$ is the cross section of the rectangular bar-shaped sample.

The polycrystalline superconductors could be considered as a weak-links array behaving like Josephson junctions. As shown in Fig. 12, the calculated J_c results show that the intergranular coupling between superconducting grains for N_2 sample is better than for the other two samples.

4 Conclusion

In conclusion, XRD and $R-T$ results show that the Nb substitution increases the volume fraction of Bi-2223 phase and normal-state resistivity of Bi-based superconductors. The broadening of the resistivity curve in the presence of external magnetic field was greater for the Nb-doped samples. We conclude that the Nb substitution decreases the flux pinning energy.

The susceptibility results show an increase in intergranular coupling and an AC loss temperature for the sample N_2 . The estimated values of critical current density confirm this result.

References

1. Wolf, F.A., Graser, S., Loder, F., Kopp, T.: Phys. Rev. Lett. **108**, 117002 (2012)
2. Lee, S., et al.: Appl. Phys. Lett. **95**, 212505 (2009)
3. Hammerl, G., Schmehl, A., Schulz, R.R., Goetzl, B., Bielefeldt, H., Schneiderl, C.W., Hilgenkamp, H., Mannhart, J.: Nature **407**, 162–164 (2000)
4. Khalil, S.M.: J. Low Temp. Phys. **143**, 112 (2006)
5. Jasiolek, G., Gorecka, J., Majewski, J., Yuan, S., Jin, S., Liang, R.: Supercond. Sci. Technol. **3**, 194 (1990)
6. Takano, M., Takada, J., Oda, K., Kitaguchi, H., Miura, Y., Ikeda, Y., Tomii, Y., Mazaki, H.: Jpn. J. Appl. Phys. **27**, 6 (1988)
7. Rose-Innes, A.C., Rhoderick, E.H.: Introduction to Superconductivity. Pergamon, New York (1978)
8. Mishra, D.R., Upadhyay, P.L., Sharma, R.G.: Physica C **304**, 293 (1998)
9. Chiu, C.W., Meng, R.L., Gao, L., Huang, z.J., Chen, F., Xue, Y.Y.: Nature **365**, 323 (1993)
10. Van Driessche, I., Buekenhoudt, A., Konstantinov, K., Bruneel, E., Hoste, S.: Appl. Supercond. **4**, 185 (1996)
11. Mazaki, H., Ishida, T., Sakuma, T.: Jpn. J. Appl. Phys. **27**, L811 (1988)
12. Kameli, P., Salamati, H., Abdolhosseini, I., Sohrabi, D.: Physica C **468**, 137 (2008)
13. Palstra, T.T.M., Batlogg, B., van Dover, R.B., Schneemeyer, L.F., Waszczak, J.V.: Phys. Rev. B **41**, 6621 (1990)
14. Kim, J.J., Lee, H., Chung, J., Shin, H.J., Lee, H.J., Ku, J.K.: Phys. Rev. B **43**, 2962 (1991)
15. Bean, C.B.: Rev. Mod. Phys. **36**, 31 (1964)
16. Ishida, T., Goldfarb, R.B.: Phys. Rev. B **41**, 8937 (1990)